Journal of Materials Chemistry A

ROYAL SOCIETY OF CHEMISTRY

PAPER

View Article Online
View Journal | View Issue

Cite this: J. Mater. Chem. A, 2026, 14, 7179

Computational and experimental insights into variable temperature propylene (C_3H_6), propane (C_3H_8), and hydrogen sulfide (H_2S) sorption in ultra-high permselectivity CANAL ladder polymers

Brandon C. Tapia, Jing Ying Yeo and Zachary P. Smith *

Membranes are a promising technology for energy-efficient separations of high-value gaseous chemical streams (*e.g.*, hydrogen sulfide from methane or propane from propylene). Among the classes of emerging microporous polymers, CANAL polymers have attracted significant interest because of their selectivities and plasticization resistance for acid gas separations. In this work, a computational atomistic system is developed for CANAL-Me-Me_2F, an archetypal CANAL polymer. Computed properties (free volume distribution, wide-angle X-ray scattering, and thermal expansion coefficients) align with experimental results. High-pressure sorption isotherms of H_2, N_2, O_2, CH_4, CO_2, H_2S, C_3H_6, and C_3H_8 were computed *via* grand canonical Monte Carlo and iterated Monte Carlo–molecular dynamics simulations, demonstrating good agreement with experimental isotherms at 35 °C. H_2S, C_3H_6, and C_3H_8 isotherms were further computed between temperatures of 55–190 °C, followed by extraction of dual-mode sorption (DMS) parameters. Sorption energetics showed less exothermic Langmuir affinity for the more polarizable gases (H_2S and C_3H_6) in CANAL-Me-Me_2F relative to PIM-1, which is ascribed to the lack of heteroatoms in CANAL-Me-Me_2F, and supported by simulations of a hypothetical nitrile-functionalized CANAL-Me-Me_2F. This study develops a computational approach that can probe the unique nanoscale behavior of CANAL polymers and applies it to studying the thermodynamics of condensable gas sorption within CANAL-Me-Me_2F.

Received 20th November 2025
Accepted 27th December 2025

DOI: 10.1039/d5ta09448h

rsc.li/materials-a

1. Introduction

Reducing energy consumption in chemical separations is an important industrial target that can address up to 15% of global energy use.[1] One potential route to achieving this goal is transitioning from conventional thermal-based separations to membrane-based systems, which leverage chemical potential gradients to separate compounds based upon their size and affinity to the membrane.[2]

Ladder polymers are a promising class of emerging materials with highly rigid and contorted backbones, among which, the best known are polymers of intrinsic microporosity (PIMs).[3] These materials have inefficient chain packing, yielding interconnected free volume elements that allow an increase in permeability while maintaining moderate selectivity.[3] Nevertheless, the out-of-equilibrium glassy structure of PIMs results in a loss of free volume with time, decreasing their permeability that would benefit industrial application.[3,4] Thus, significant work has been devoted to developing microporous membranes that can mitigate physical aging.[3]

In 2022, Lai *et al.*[5] reported a class of 3D-contorted ladder polymers made *via* catalytic arene–norbornene annulation (CANAL) polymerization, comprised of fused norbornyl benzocyclobutene repeat units. These CANAL polymers exhibited molecular weights between 67 and 170 kDa, suitable for forming mechanically and thermally robust gas separation membranes. Interestingly, CANAL polymers exhibit a unique physical aging trend that does not follow the upper bound relationship. Instead, selectivity is greatly increased while permeability does not suffer significantly for small molecules, unlike the commonly observed tradeoff in other membrane materials, including traditional PIMs.[3,6] This aging behavior allows for CANAL polymers to rival industrially used membranes in selectivity while significantly surpassing them in permeability. For example, the CANAL polymer studied in this work, CANAL-Me-Me_2F, exhibits twice the selectivity and 100 times the permeability of industrial cellulose acetate membranes for CO_2/CH_4 separations after 150 days of aging.[5]

Considering these prior promising results, this study examines sorption of gas streams containing propylene (C_3H_6) and propane (C_3H_8), and hydrogen sulfide (H_2S) in CANAL-Me-Me_2F. These gases were selected due to their industrial relevance and the typical challenges in accessing experimental data

Department of Chemical Engineering, Massachusetts Institute of Technology, Cambridge, Massachusetts 02139, USA. E-mail: zpsmith@mit.edu

for these gases. Propylene is an essential feedstock for plastic production, but the generation of propylene, largely *via* thermal cracking, also generates propane which must be removed.[1,7,8] This separation is challenging due to similar boiling points (C_3H_6: −47.62 °C, C_3H_8: −42.11 °C) and van der Waals diameters (C_3H_6: 4.0 Å, C_3H_8: 4.2 Å) of the gases, leading to a highly energy-intensive distillation process.[9–11] Hydrogen sulfide is another component that must be removed from hydrocarbon streams due to both its toxicity and ability to poison catalysts, especially as lower-quality feedstocks become economically feasible.[12] Industrially mature fuel-gas sweetening relies on either cryogenic distillation or absorption depending on the target application (*i.e.*, liquid or gaseous product).[13,14] However, these methods must overcome enthalpies of condensation or leverage toxic solvents during operations, respectively. These unwanted features are not found in membrane separations.[1,15,16]

Due to the exceptional microporosity of CANAL polymers, which exhibit some of the highest BET surface areas of polymers reported in literature, they are expected to exhibit high sorption capacities despite their lack of heteroatoms.[5] However, sorption studies on olefins, paraffins, and acid gases, while highly desirable, remain limited in the open literature.[17,18] To the best of our knowledge, there has only been one study by Yeo *et al.*[19] focusing on H_2S separations in CANALs, and none focusing on olefin/paraffin applications. Moreover, H_2S-focused studies are also limited for the archetypal PIM (PIM-1) and its derivatives.[20–23] There are likely two main reasons for this lack of H_2S-focused work in the literature: (1) H_2S is a highly toxic gas, limiting capabilities in academic labs to consider these experiments, and (2) gathering experimental sorption data is time consuming, especially for gases such as H_2S and condensable hydrocarbons with high sorption capacity. Additionally, many experimental systems are limited to temperature ranges that may be inadequate for industrial applications. Nevertheless, these studies are necessary to understand the thermodynamic behavior of these complex mixtures and to evaluate their potential in gas separations, especially as sorption selectivity can be more indicative of membrane performance relative to diffusion selectivity for highly sorbing gases, such as H_2S-containing mixtures.[17] Specifically, sorption analyses help to characterize polymer–gas affinity, predict effects of competitive sorption, and quantify polymer–gas energetics. As a result, these measurements are vital tools that can be used to investigate whether CANALs are a feasible materials platform for various gas separations.

Simulations provide an important complement to experiments. They can probe nanostructure relationships and conditions inaccessible to experimental methods, and can provide high throughput studies to identify promising candidates for future experimental synthesis and studies. In an effort to add to the presently limited literature on sour gas and olefin/paraffin separations in high free volume polymers, we present here a combined experimental and computational study of C_3H_6, C_3H_8, and H_2S sorption within CANAL-Me-Me$_2$F.

We validate this framework by first comparing our results to experimentally measured properties (density, wide-angle X-ray scattering, free volume distribution, and sorption isotherms), followed by simulating properties that are potentially experimentally inaccessible, namely sorption and associated energetics for C_3H_6, C_3H_8, and H_2S at temperatures of 35 °C, 55 °C, 125 °C, and 190 °C.

2. Background and theory

The sorption–diffusion model is commonly applied to describe gas transport in polymeric membranes, where P is the permeability, D is the effective diffusion coefficient, and S is the effective sorption coefficient:[2]

$$P = D \times S \tag{1}$$

The sorption coefficient can be calculated from sorption experiments as

$$S = \frac{C}{f} \tag{2}$$

where C is the concentration of gas sorbed ($cm_{STP}^3\ cm_{pol}^{-3}$) in the membrane in equilibrium with the gas phase at fugacity f (atm). Pure-gas sorption in glassy polymers is frequently modeled *via* the dual-mode sorption (DMS) model:[24–26]

$$C = k_D f + \frac{C_H' b f}{1 + b f} \tag{3}$$

where k_D is Henry's constant ($cm_{STP}^3\ cm_{pol}^{-3}\ atm^{-1}$), C_H' is the Langmuir capacity constant ($cm_{STP}^3\ cm_{pol}^{-3}$), and b is the Langmuir affinity constant (atm^{-1}). The DMS model views sorption in a polymer as the simple addition of sorption in hypothetical Langmuir and Henry modes, which are said to dominate partitioning at low and high pressures, respectively.[24]

The sorption selectivity ($\alpha_{i/j}^S$) for one gas over another is defined by the ratio of their respective sorption coefficients:

$$\alpha_{i/j}^S = \frac{S_i}{S_j} = \frac{C_i}{f_i} \Big/ \frac{C_j}{f_j} \tag{4}$$

Ideal sorption selectivity refers to the sorption selectivity calculated based on the ratio of the pure-gas sorption coefficients. However, attempting to infer mixed-gas sorption from pure-gas experiments is challenging, especially for condensable gases, which not only preferentially exclude less condensable gases from sorbing but also plasticize the polymer matrix.[17,19] One method to address this behavior is by using the adjusted DMS model by Koros *et al.*,[27] who extended the applicability of the DMS model to predict mixed-gas sorption of component i in an n-component mixture from pure-gas sorption data by accounting for competition between penetrants for a finite region of Langmuir sorption:

$$C_{i,\text{mixed}} = k_{D,i} f_i + \frac{C_{H,i}' b_i f_i}{1 + b_i f_i + \ldots + b_n f_n} \tag{5}$$

As there may be multiple solutions to the DMS model with similar goodness of fits as shown by Ricci *et al.*,[28] extracting physically meaningful results from the parameters requires

additional constraints within the optimization procedure. One class of constraints are linear free energy relationships (LFERs) and Van't Hoff relationships applied to the DMS fitting procedure as performed by Wu *et al.*[29]

In the limit of infinite dilution, sorption can be decoupled into Langmuir and Henry mode sorption as:

$$S_\infty = \lim_{f\to 0}\frac{C_i}{f_i} = S_{\infty,\text{Henry}} + S_{\infty,\text{Langmuir}} = k_{\text{D},i} + C'_{\text{H},i}b_i \quad (6)$$

As sorption is an equilibrium process, it can be further described *via* a Gibbs free energy relationship and subsequently separated into an entropic prefactor ($S_{\infty,0}$) coupled with an enthalpic Van't Hoff temperature dependence:

$$S_\infty = S_{\infty,0}\exp\left(-\frac{\Delta H_{S,\infty}}{RT}\right) \quad (7)$$

where $\Delta H_{S,\infty}$ is the infinite dilution heat of sorption.[29–31] Likewise, the same approach can be applied to the Henry and Langmuir sorption modes independently to extract the heats of Henry sorption (ΔH_D)

$$k_\text{D} = k_{\text{D},0}\exp\left(-\frac{\Delta H_\text{D}}{RT}\right) \quad (8)$$

and Langmuir sorption (ΔH_b)

$$b = b_0\exp\left(-\frac{\Delta H_\text{b}}{RT}\right) \quad (9)$$

where $k_{\text{D},0}$ and b_0 are again entropic prefactors.[29,32]

3. Computational methods

3.1 Simulated polymerization technique

Simulating polymer structures to extract physically meaningful property sets is challenging, primarily due to their amorphous nature and the limited chain lengths that can be accessed with simulations.[33] Unlike crystalline and other ordered structures (*e.g.*, metal–organic frameworks), amorphous polymers do not have periodic structures that can be readily compiled. Ladder polymers and PIMs bring the additional challenge of high steric hindrance due to their bulky structures.[34] Thus, traditional polymer building methods such as random walks, reverse Monte Carlo (RMC), or configurational bias Monte Carlo (CBMC) methods frequently fail to properly reduce the energy of the system or reproduce experimentally observed steric hindrance.[33,34] To overcome these issues, simulated polymerization was employed here using the open-source Polymatic polymerization algorithm and software (version 1.1).[33,35] Briefly, the Polymatic technique places all monomers within a simulation box. Next, attempts are made to find bonding candidates based upon distance and orientation between potential bonding atoms. Should no candidates for polymerization be found, molecular dynamics are employed to search for more favorable bonding positions. Polymatic is extensively described in literature and has been validated with multiple polymers, including the archetypal microporous polymer, PIM-1.[33,34,36–39]

The standard energy minimization strategy within the Polymatic algorithm was employed where canonical (NVT) molecular dynamics were performed every 5 polymerization steps except for when isothermal–isobaric (NPT) molecular dynamics were employed every 15 polymerization steps.[33] Additional bonding orientation constraints were employed to reduce unrealistic bond generation. Artificial charges of ±0.3 e were added to bonding atoms to increase bonding probability but removed once bonding was finalized. These orientation constraints and artificial charges are built into Polymatic and have been used previously for PIM-1.[33]

3.2 Polymer relaxation

After polymerization, CANAL-Me-Me$_2$F underwent a molecular dynamics relaxation scheme to more closely reflect its morphology under experimental conditions. To achieve this result, a 21-step equilibration algorithm was used where the pressure was stepped up in increments and then gradually reduced (Fig. S1 and Table S1) as recommended by Abbot *et al.*[33] This 21-step technique was developed based on the initial work of Theodorou and Suter and modified by Larsen *et al.*[34,40] Molecular dynamics were performed with LAMMPS (version 22 Aug 2018 for pre-processing steps and version 28 Mar 2023 for sorption isotherms).[41]

3.3 Simulation parameters

Two separate systems were developed. The first was a united-atom (UA) framework defined by the General Amber Force Field 2 (GAFF2) force field for intramolecular energies and the Transferable Potential for Phase Equilibria United-Atom (TraPPE-UA) force field for intermolecular energies as was previously shown to apply well for PIMs.[33,36–38,42–48] In this UA technique, hydrogens are coupled with their respective heavy atoms, forming pseudoatoms. The second system was an all-atom (AA) framework defined by the GAFF2 force field for both inter- and intramolecular energies.[45] Partial charges were generated using the restrained electrostatic potential (RESP) approach at the HF/6-31G(d) level using the Connolly surface algorithm in Gaussian 16 *via* the PyRed program.[49–53] To quantify charges, a single repeat unit model was used, except on bonding atoms where two joined repeat units were used instead so that the charges on bonding atoms could be better described. This method of using polymer periodicity has been previously applied in charge fitting and force field parameterization as polymers are generally too large to feasibly fit quantum-mechanically-derived charges to the entire chain.[42,54–56] Charge tail corrections were included up to 15 Å and cross-charges were calculated using the Lorentz–Berthelot mixing rules.[57] The particle–particle–particle mesh (PPPM or P3M) method with a desired relative error ("accuracy") of 10^{-5} was used to calculate long-range Coulombic interactions.[58] A Nosé–Hoover thermostat and barostat[59–62] were employed with Størmer–Verlet integration.[63,64] All penetrants except for H_2 and H_2S used the GAFF2 and TraPPE-UA force fields for inter- and intramolecular parameters, respectively. The H_2 force field was modeled using the parameters of Yang and Zhong,[65] as suggested for use by Barraco *et al.*[66] The H_2S force field was modeled using a modified 4–3 model originally developed by Shah *et al.*[67] Additional

information on the H_2S force field is available in Section S1.3 of the SI.

3.4 Fixed and flexible adsorption techniques

Grand canonical Monte Carlo (GCMC) simulations were employed to generate sorption isotherms using the Cassandra Monte Carlo package (version 1.2.6).[68] GCMC holds chemical potential (μ), volume (V), and temperature (T) constant. Both a rigid and a flexible method were employed for sorption isotherm generation. The rigid method solely employed GCMC with the polymer system held static throughout the run. These rigid simulations were run for 2 000 000 MC steps with the final one-third of the data used to calculate equilibrium averages (Fig. S3). The flexible method employed iterative MC and MD (MCMD), where one iteration consisted of 2 000 000 MC steps followed by 2 ns of isothermal–isobaric MD with a 0.5 fs timestep to allow for system relaxation. All inserted gas molecules were intramolecularly fixed (*i.e.*, no bending or stretching) but were allowed to rotate and translate during MD. The 0.5 fs timestep was used to account for this rigid adsorbate assumption as reported previously.[37] Each flexible isotherm was run for at least 5 cycles at each pressure point, but cycles were continued until they converged (Fig. S4 and S5 and Table S2). To achieve these flexible simulations, communication between LAMMPS and Cassandra was performed with the Python-based pysimm package (using an in-house modified distribution of version 1.1, both of which are open-source).[69–73] The flexible method provides a more realistic system description of condensable gas uptake by allowing molecular rearrangement, but it is significantly more computationally expensive than the rigid method.

3.5 Uncertainty and error propagation

As CANAL-Me-Me_2F is amorphous, five different systems were generated independently using Polymatic. Uncertainties in "static" properties (*i.e.*, properties that were directly calculated from the equilibrated polymer system, *e.g.*, density) were determined as the sample standard deviation between the five replicates. Uncertainties in Monte Carlo simulations were determined as the sample standard deviation of the fluctuations within each replicate's equilibrium value, followed by error propagation between the five replicates.[74]

3.6 Gravimetric and volumetric sorption

Depending on the study, results may be reported gravimetrically (*e.g.*, mmol g^{-1}) or volumetrically (*e.g.*, cm_{STP}^3 cm_{pol}^{-3}) where conversion between the two is described as follows:

$$C = 22.414 \frac{cm_{STP}^3}{mmol} \cdot q \cdot \rho_{pol} \quad (10)$$

where C is the volumetric concentration (cm_{STP}^3 cm_{pol}^{-3}), q is the gravimetric loading (mmol g^{-1}), and ρ_{pol} is the polymer density (g cm^{-3}). Preference between the two forms is largely dependent on the material form factor and the experimental techniques for measurements. For *in silico* studies, results have been reported using both methods.[36,75]

While both methods are reasonable, challenges arise when attempting to compare computationalto experimental results. Since the polymer density within the simulation may not match that of experiment, as has been previously shown by Abott *et al.*[33] for PIM-1, the conversion between measurement styles can influence comparison between simulated and experimental results. To account for this density difference, the simulated volumetric results reported here are scaled by the ratio of experimental to simulated densities, effectively normalizing the results so that they are comparable regardless of measurement style reported. In other words, the ρ_{pol} used in eqn (10) is the experimental density, not the simulated density.

4. Experimental methods

4.1 Density measurements

CANAL-Me-Me_2F films were solution cast and subject to methanol treatment using the same procedure described in Lai *et al.*[5] The density of the films was measured using a gravimetric approach, and the area was determined using a hand-traced polygon in ImageJ software (version 1.51 k).[76] The thickness across the films was measured using a Mituyo (Kanagawa, Japan) micrometer, with an accuracy of $\pm$ 1.27 μm.

4.2 Free volume distribution *via* non-local density functional theory (NLDFT)

BET surface areas of the CANAL-Me-Me_2F polymers were measured with an N_2 probe at 77 K using a Micromeritics ASAP 2020 with the same procedure as described in Lai *et al.*[5] Analysis of free volume distributions was performed using the non-local density functional theory (NLDFT) model for carbon slit pore geometry using the SAIEUS software, which implements the L-curve method for the regularization parameter, λ.[77]

4.3 Experimental gas sorption isotherm measurements

Gas sorption isotherms for the CANAL-Me-Me_2F films were collected using an automated constant-volume pressure-decay system from Maxwell Robotics (Austin, TX) at 35 °C. A detailed protocol for these tests can be found in previous work by Mizrahi Rodriguez *et al.*[78]

4.4 Thermal expansion coefficient *via* dynamic mechanical analysis (DMA)

To understand the dimensional change in the CANAL-Me-Me_2F films during heating, the length of each film was continuously measured using a single screw film clamp test experiment on a TA Instruments (New Castle, DE) DMA 850 using a heating (30 to 140 °C) procedure with a ramp rate of 5 °C min^{-1}.

4.5 Materials

Chloroform (HPLC grade) and methanol (ACS reagent grade) were purchased from Sigma Aldrich (St. Louis, MO). The following gases were purchased from Airgas (Radnor, PA): He (>99.999%), H_2 (>99.999%), N_2 (>99.999%), O_2 (>99.999%), CH_4 (>99.99%), H_2S (air certified standard mixture, 99.99%), C_3H_6

(>99.0%), and C_3H_8 (>99.0%). CANAL-Me-Me$_2$F polymer used for C_3H_8 and C_3H_6 sorption and density measurements was purchased from Osmoses (Cambridge, MA). CANAL-Me-Me$_2$F polymer used for H_2, O_2, N_2, and CH_4 sorption is the same polymer as previously studied by Lai *et al.*[5]

5. Results and discussion

5.1 System validation

The chosen molecular system parameters were validated *via* structural property alignment between simulated and experimental systems. To make this validation, bulk density, skeletal density, free volume distribution (FVD), and the static structure factor of the simulated system were determined.

Bulk density is defined as

$$\rho_{\text{bulk}} = \frac{m}{V_{\text{tot}}} \tag{11}$$

where m is the system's total mass and V_{tot} is the system volume, including void space. Skeletal density, ρ_{skel}, is the density of the system with the void volume, V_{void}, removed:

$$\rho_{\text{skel}} = \frac{m}{V_{\text{skel}}} = \frac{m}{V_{\text{tot}} - V_{\text{void}}} \tag{12}$$

Skeletal densities were calculated using PoreBlazer (version 4.0)[79] with a helium probe (d = 2.60 Å) and mapping *via* the Connolly surface algorithm, as done previously by Abbot *et al.* for PIM-1.[35,53,80]

The experimental bulk density at room temperature of 0.96 ± 0.02 g cm^{-3} led to differences of 17% and 1% compared to the bulk densities of the UA and AA frameworks at 35 °C, respectively. Abbot *et al.*[35] reported simulated bulk densities for UA frameworks consistently lower than experimental bulk densities for multiple polymers (PS, PMMA, PET, PC, PEI, PIM-1) when polymerized with Polymatic, hypothetically due to difficulty in comparing geometrically- and experimentally-derived densities, especially for high free volume polymers, where differences are likely amplified.

The simulated bulk density of the polymer decreases with increasing temperature for both the UA and AA frameworks as shown in Fig. 1. Interestingly, the slopes of the density *versus* temperature plots for both the UA and AA frameworks are remarkably similar at $(-2.2 \pm 0.2)\cdot10^{-4}$ g cm^{-3} K^{-1} and $(-2.3 \pm 0.2)\cdot10^{-4}$ g cm^{-3} K^{-1}, respectively for bulk density. Free volume theory predicts that an increase in free volume should increase the volumetric thermal expansion coefficient, α_V, defined as:[81]

$$\alpha_V = \frac{1}{V}\left(\frac{\partial V}{\partial T}\right)_P = -\frac{1}{\rho}\left(\frac{\partial \rho}{\partial T}\right)_P \approx -\frac{1}{\rho_0}\frac{\Delta\rho}{\Delta T} \tag{13}$$

where the approximation is valid for $\Delta\rho/\rho_0 \ll 1$ (eqn S2–S5). However, we hypothesize that our findings are due to both the UA and AA frameworks attempting to simulate the same underlying physical mechanisms. In other words, even though the frameworks' respective geometries create different equilibrium packing, the effect of temperature remains consistent across both frameworks. This hypothesis is further supported by noting that both AA[82–84] and UA[84–87] models are frequently employed to explore the thermal behavior of amorphous polymers in both their rubbery and glassy regimes. The "macroscopic"[88] nature of examining density as a function of temperature may obfuscate any significant temperature-dependent differences that arise due to free volume discrepancies between UA and AA models, which may be occurring on a more microscopic scale. The data is also represented as the change in fractional free volume (FFV) with temperature in Fig. S8.

The experimental volumetric thermal expansion coefficient was determined from the linear thermal expansion coefficient (α_L) and, assuming isotropic expansion, calculated as:[89]

$$\alpha_V = 3\alpha_L \tag{14}$$

The α_V for both simulated and experimental systems is shown in Table 1. Two temperature ranges were selected for the simulated systems: one range that better aligns with the experimental data, and a second broader range to provide a value with reduced error by increasing the number of datapoints used. Both experimental and simulated results fall within the same order of magnitude and error. As one might expect based on their similar temperature dependence, the UA and AA systems have similar expansion coefficients. The experimental DMA expansion data is shown in Fig. S6. While the bulk density changes with temperature, the skeletal density

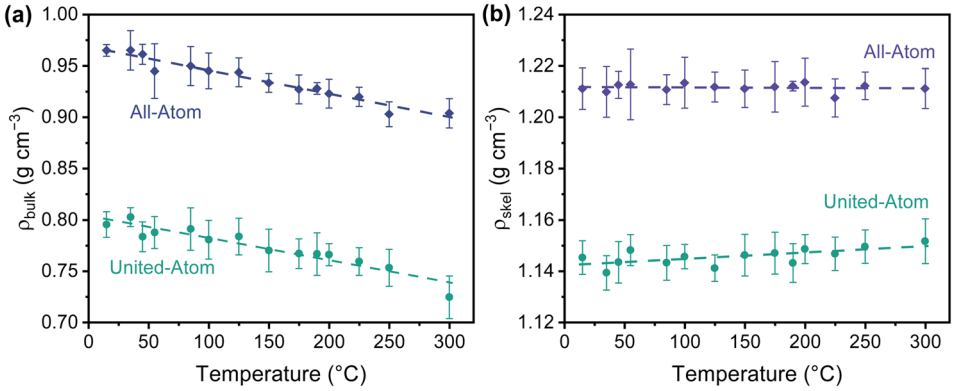

Fig. 1 (a) Bulk and (b) skeletal densities *versus* temperature of simulated CANAL-Me-Me$_2$F for all-atom (AA) and united-atom (UA) frameworks. Dashed lines show linear regressions. Error bars represent uncertainty as the standard deviation over five independent CANAL-Me-Me$_2$F systems.

Table 1 Volumetric thermal expansion coefficients (α_V) for simulated and experimental systems compared to select glassy polymers

System	Polymer	α_V ($10^4 \cdot K^{-1}$)	Temperature range (°C)
United-atom	CANAL-Me-Me$_2$F	2.2 ± 0.8	35–150
		2.7 ± 0.3	15–300
All-atom	CANAL-Me-Me$_2$F	2.3 ± 0.6	35–150
		2.4 ± 0.2	15–300
Experimental	CANAL-Me-Me$_2$F	1.0–2.2[a]	35–139
Experimental[90]	Polystyrene	1.8–2.4	$<T_g$
Experimental[90]	poly(methyl methacrylate)	2.1	$<T_g$
Experimental[91]	Cellulose acetate	3.3[b]	$<T_g$
Experimental[92]	PIM-1	2.1	30–110

[a] As further explained in Section S2.1, the experimental α_V was found using a polynomial fit, creating a non-constant value. [b] Reference provided α_V, thus, eqn (14) was not applied.

is nearly constant within uncertainty with temperature (skeletal density linear regressions: $(2.5 \pm 0.8)\cdot10^{-5}$ g cm^{-3} K^{-1} and $(-2 \pm 5)\cdot10^{-6}$ g cm^{-3} K^{-1}, respectively, for UA and AA systems). This phenomenon indicates that the increase in temperature is increasing the void space between polymer chains with limited effect on the skeletal structure.

To better understand the polymer microstructure, the FVD was calculated using PoreBlazer, defined as the negative derivative of the cumulative free volume, V, with respect to the probe diameter, D:

$$\mathrm{FVD} \equiv -\frac{\mathrm{d}V(D)}{\mathrm{d}D} \quad (15)$$

The FVD is also commonly referred to as the pore size distribution (PSD), including within PoreBlazer, however, FVD is used here to distinguish the micropores within these polymers from more classically defined porous materials. As the location of atoms is required, this geometric FVD method is only applicable to simulated systems. Experimental FVD determination relies on indirect methods such as NLDFT[39,93,94] or positron annihilation lifetime spectroscopy (PALS).[95,96] Fig. 2a compares experimentally determined FVD *via* NLDFT to geometric FVD using a helium probe ($d = 2.60$ Å)[80] which reveals significant differences between the two methods. To ensure differences between probe size and/or temperature were not significantly altering the geometric FVD, a nitrogen ($d = 3.64$ Å)[80] probe was also considered for simulations at 77 K and 308 K (Fig. S7). These results are in agreement with a previous study by Kupgan *et al.*,[39] which showed NLDFT to systematically overpredict free volume elements (FVEs) for amorphous polymers, including PIM-1. When considering the impressive ability for microporous organic polymers, including CANAL-Me-Me$_2$F, to selectivity separate gases below diameters of 4 Å, it is further evidence of FVD overprediction using NLDFT methods, as these methods predict all FVEs to be larger than 4 Å.[5,19] Fig. 2b and c detail the minimum and maximum pore sizes present, taken as the values at which 99% and 1% of the cumulative free volume was accessible, respectively, over a 15–300 °C temperature range. The AA framework shows a narrower FVD than the UA framework across all temperatures. The FVD is seen to broaden with increasing temperature—largely due to the increase in the maximum FVE size, which increases an order of magnitude faster than the minimum FVE size. These results agree with the density decreasing as a function of temperature, as free volume elements may increase in size as the polymer expands. The more uniform minimum FVE size with increasing temperature suggests that even though the average FVE size may increase, there remain stochastically fluctuating pockets that maintain gas sieving capabilities even at high temperatures.

Crystallographic data was computed using the Interactive Structure Analysis of Amorphous and Crystalline Systems (ISAACS) program (version 2.10).[97] The static structure factor, $S(q)$, was used to compare against experimental wide-angle X-ray scattering (WAXS) data from Lai *et al.*[5] The simulated scattering data reasonably follows the experimentally gathered data with a broad amorphous halo around 1.0 Å^{-1} as shown in Fig. 3. The d-spacing for the amorphous halo of the experimental results is 7.1 Å, while that of the UA and AA results are 6.6 Å and 6.5 Å, respectively. For the experimental result, the increase in intensity as q goes to zero is not visible in the simulated static

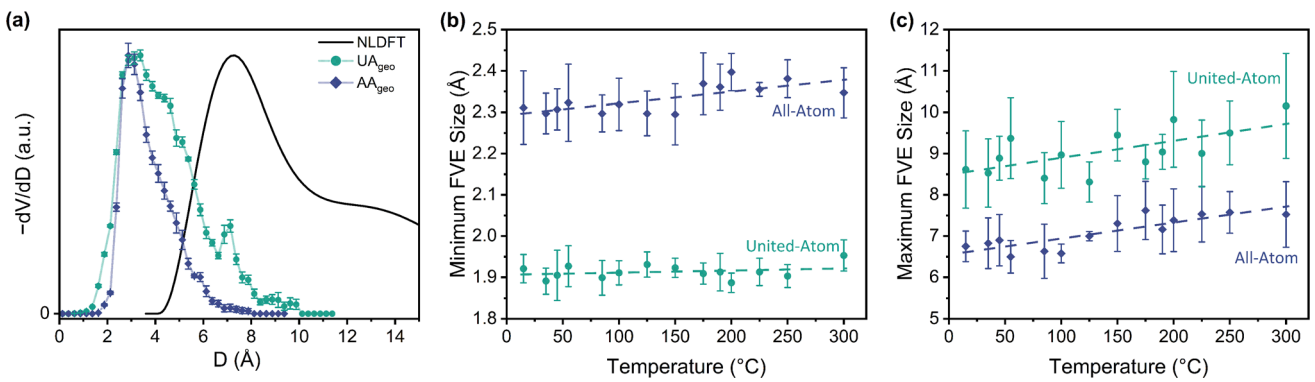

Fig. 2 (a) Free volume distributions (FVDs) of CANAL-Me-Me$_2$F from non-local density functional theory (NLDFT) *via* experimental N_2 sorption measurements at 77 K as well as simulated geometric determination from united-atom (UA) and all-atom (AA) simulations at 35 °C using a helium probe. Solid lines are meant to guide the eyes. Data are normalized to their maximum ordinate value. (b) Minimum and (c) maximum FVEs present in the UA and AA CANAL-Me-Me$_2$F frameworks across a temperature range of 15–300 °C. Dashed lines show linear regressions.

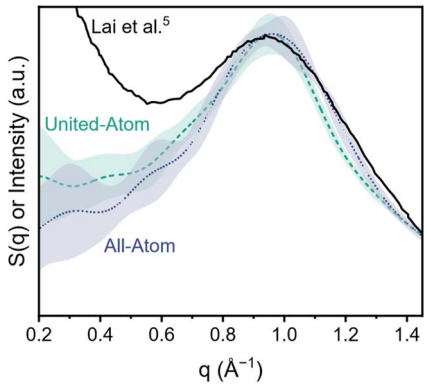

Fig. 3 Experimental wide-angle X-ray scattering (WAXS) data (solid line) from Lai *et al.*[5] compared with simulated static structure factors of all-atom (dotted line) and united-atom (dashed line) CANAL-Me-Me_2F systems. Error bands represent the sample standard deviation from five replicate polymer systems. Data are normalized to their maximum ordinate value in the range 0.9–1.1 Å^{-1}.

structure factor and is attributed to experimental error as the regime around and below 0.3 Å^{-1} is better suited for small-angle X-ray scattering (SAXS).[98]

5.2 Small-gas sorption isotherms

This study focuses primarily on H_2S, C_3H_6, and C_3H_8, which are plasticizing gases. When compared to smaller gases, such as H_2 and N_2, these larger gases create complexities with modeling, such as the need for additional force field parameters and iterated MCMD. To better understand limitations specific to the polymer model itself, sorption isotherms for fixed-framework UA models of H_2, N_2, O_2, and CH_4 were simulated at 35 °C and compared to experimentally obtained sorption isotherms, shown in Fig. 4. Because these smaller gases do not cause detectable polymer plasticization, flexible frameworks do not provide increased convergence with experimental results, as shown explicitly in Fig. 4a and d for H_2 and CH_4, respectively.

The simulated systems show quantitative agreement with experimental results. Specifically, results for H_2, N_2, and O_2 fall within error of experimental values, while results for CH_4 show slight under- or overprediction depending on whether an MC or MCMD procedure was applied. The usage of a flexible framework increases the sorbed concentration of a gas when compared to the rigid framework, as polymer rearrangement within the flexible framework allows gas molecules to settle in previously inaccessible locations. These results indicate the ability for the CANAL-Me-Me_2F model to quantitatively model sorption using GCMC for non-plasticizing gases and give credence to the relevance of the chosen forcefield parameters. The ability to model experimental isotherms agrees with previous studies that have found GCMC to be a valuable tool for predicting sorption of non-plasticizing gases in polyimides, porous aromatic frameworks, and PIMs.[34,100,101]

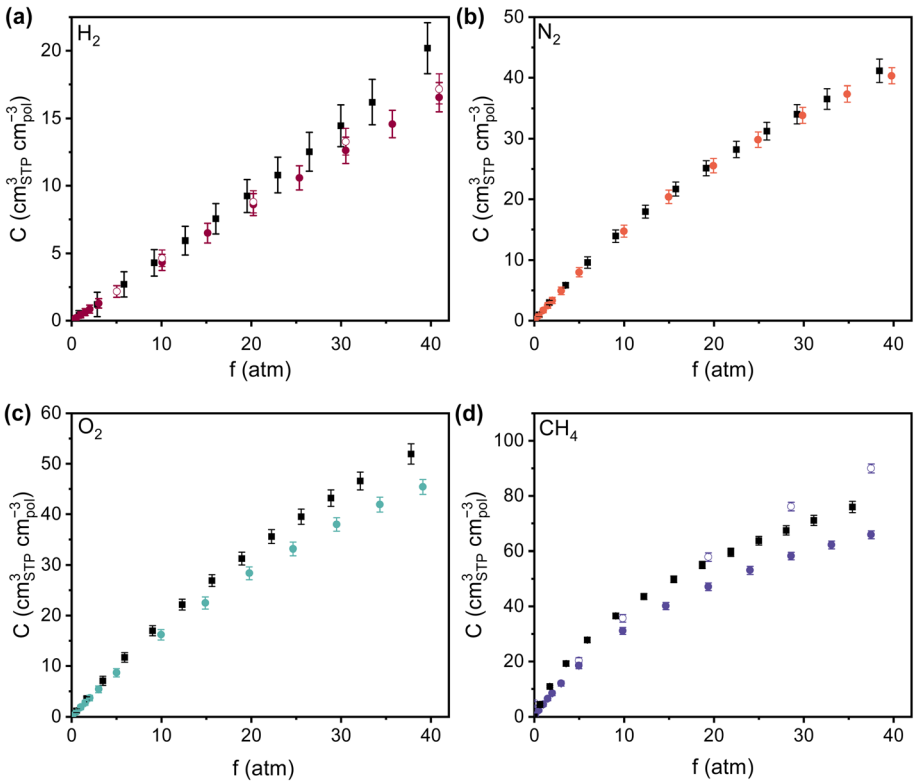

Fig. 4 Comparisons of united-atom simulations and experimental (black squares) isotherms in CANAL-Me-Me_2F for (a) H_2, (b) N_2, (c) O_2, and (d) CH_4, all at 35 °C. Rigid (filled datapoints) and flexible (unfilled datapoints) isotherms were computed for H_2 and CH_4 while only rigid isotherms were computed for N_2 and O_2. Fugacity was calculated *via* a second-order Virial expansion.[99]

5.3 Plasticizing gas sorption isotherms

For plasticizing gases (*e.g.*, CO_2, H_2S, C_3H_6, and C_3H_8), the effects of fixed *versus* flexible framework were significant, as exemplified in Fig. 5. For CO_2, the flexible framework overpredicted yet showed qualitative agreement with experimental results at fugacities below 20 atm before strongly diverging. Interestingly, for CO_2, the flexible framework performed worse than the fixed framework. The flexible framework model for H_2S underpredicted yet qualitatively aligned with the experimental H_2S isotherm at fugacities below 10 atm. For the larger C_3H_6 and C_3H_8 hydrocarbons, quantitative agreement with experimental isotherms is demonstrated at low to moderate fugacities (<3 atm), indicating the applicability of this flexible framework. These comparisons with experimental results highlight how the polar molecules (CO_2 and H_2S) show poorer alignment with experimental results than the hydrocarbons. This result could be due to the additional force field complexities that arise for interparticle interactions when significant polarity is present, amplifying the relative simplicity of force fields compared to actual molecular electronic behavior. Therefore, even for plasticizing gases, it is advisable to compare both fixed and flexible frameworks to determine which is best for specific cases.

Previous studies that have examined CO_2 sorption in PIM-1 using the iterative MCMD approach have reported both under- and overfitting, compared to experimental results.[37,104] The broad range of CO_2 sorption isotherms in PIM-1 is indicative of the fact that slight changes in reaction conditions, post-treatment, and testing methods can significantly alter the results.[105] Compounding these challenges is the issue that simulated "synthesis," relaxation, and sorption measurements are unable to be performed as one would do experimentally. Thus, we emphasize that divergence from experimental results is not unexpected given these limitations and experimental scatter.[106]

5.4 Dual-mode sorption model

An LFER and Van't Hoff constrained DMS model has previously been applied to CANALs and H_2S sorption in glassy polymers.[19,22] Here, we extend those H_2S results reported at 35 °C to 35–190 °C. Sorption isotherms and their corresponding DMS fits are shown in Fig. 6 with DMS parameters tabulated in Table 2. As the effect of Langmuir sorption decreases with increasing temperature due to the deactivation of surface modes and the exothermic nature of Langmuir sorption, the sorption isotherms become more linear with increasing temperature. Details on the DMS fitting procedure including initial guesses and parameter bounds (Tables S4–5) are available in the SI.

In the optimization, no functional form was fit to the Langmuir capacity constant C'_H, as it has previously been fit to both linear[107] and Van't Hoff temperature dependent models,[32] as shown in eqn (16) and (17), respectively:

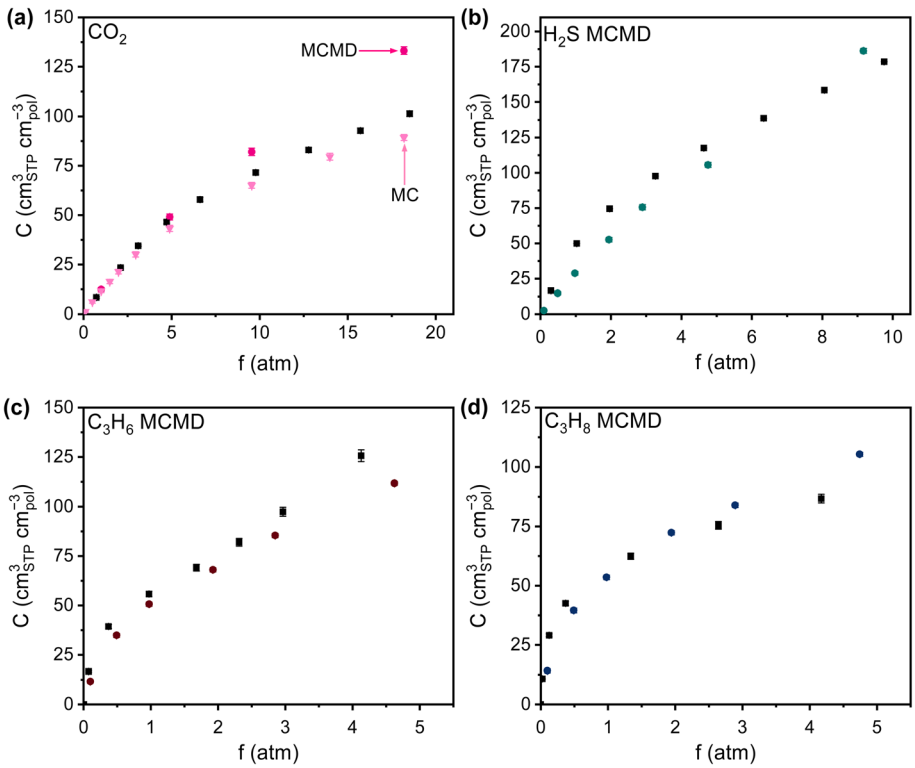

Fig. 5 Comparison of flexible framework united-atom simulations and experimental isotherms in CANAL-Me-Me_2F at 35 °C for (a) CO_2, (b) H_2S, (c) C_3H_6, and (d) C_3H_8. Experimental results are shown with black squares while flexible framework (MCMD) simulations are shown with colored circles. Fixed framework united-atom simulations are shown for CO_2 in (a) as triangles. Fugacity was determined for CO_2, C_3H_6 and C_3H_8 *via* a second-order Virial expansion and for H_2S with the Peng–Robinson equation of state.[99,102,103] The experimental H_2S isotherm has previously been reported in Yeo *et al.*[19]

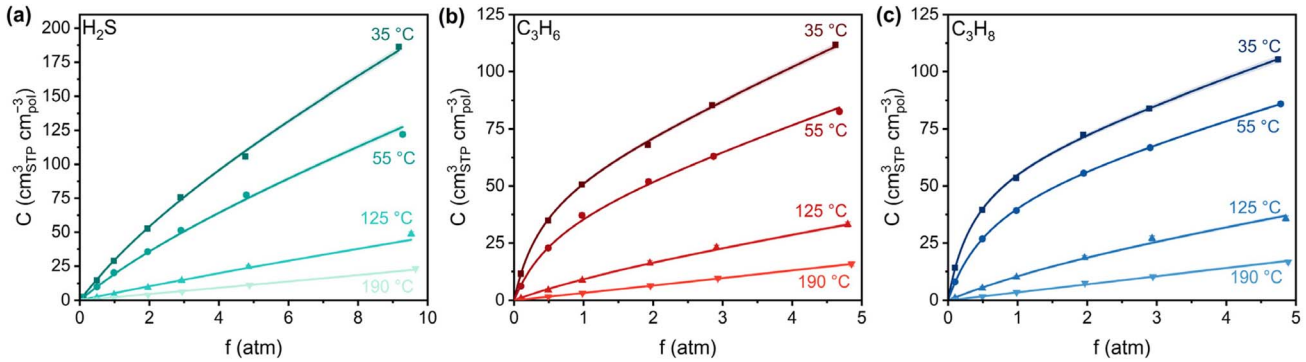

Fig. 6 Simulated MCMD sorption isotherms and corresponding dual-mode sorption (DMS) model fits for (a) H_2S, (b) C_3H_6, and (c) C_3H_8 at temperatures of 35 °C, 55 °C, 125 °C, and 190 °C. DMS fits were restricted *via* linear-free energy relationships (LFERs) and Van't Hoff constraints as implemented by Wu *et al.*[29] Uncertainties in DMS parameters were estimated from the inverse of the Hessian of χ^2 at the optimum, followed by standard error propagation to determine uncertainty in concentration.[74]

Table 2 Dual-mode sorption parameters for CANAL-Me-Me_2F, fit using an LFER-constrained model[29]

Gas	Temperature (°C)	k_D (cm_{STP}^3 cm_{pol}^{-3} atm^{-1})	C'_H (cm_{STP}^3 cm_{pol}^{-3})	b (atm^{-1})
H_2S	35	13.7 ± 0.2	87 ± 3	0.223 ± 0.002
	55	9.9 ± 0.1	54 ± 2	0.210 ± 0.005
	125	4.12 ± 0.03	8 ± 2	0.18 ± 0.02
	190	2.32 ± 0.01	0.0 ± 0.5	0.16 ± 0.03
C_3H_6	35	13.5 ± 0.2	53 ± 1	2.40 ± 0.04
	55	10.4 ± 0.1	40.5 ± 0.4	1.60 ± 0.01
	125	5.2 ± 0.1	12 ± 1	0.54 ± 0.03
	190	3.3 ± 0.1	0.0 ± 0.7	0.26 ± 0.02
C_3H_8	35	10.2 ± 0.2	61 ± 1	2.64 ± 0.05
	55	8.4 ± 0.1	51.7 ± 0.6	1.58 ± 0.01
	125	5.0 ± 0.1	20 ± 1	0.39 ± 0.01
	190	3.5 ± 0.1	0 ± 1	0.16 ± 0.01

$$C'_{H,j} = \alpha_{1,j} + a_{2,j}T \quad (16)$$

$$C'_{H,j} = \beta_{1,j}\exp\left(-\frac{\beta_{2,j}}{RT}\right) \quad (17)$$

where $\alpha_{i,j}$ and $\beta_{i,j}$ are fitting parameters for gas j. The DMS results presented here allow for an analysis of the C'_H parameter from the LFER-constrained DMS model across a large range of temperatures. As shown in Fig. 7, both models show similar goodness-of-fit. The log-modified mean absolute percentage error (MAPE)[108] for each model is shown in Table 3, indicating that the more applicable model in a given scenario is dependent on the specified gas and temperature. However, when extrapolating towards $C'_H = 0$ to approximate where Langmuir sorption is no longer present, the proposed Van't Hoff relationship significantly overpredicts the corresponding temperatures

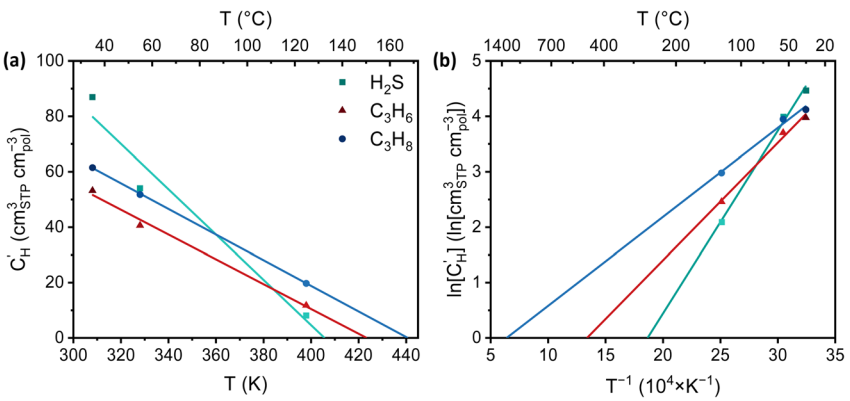

Fig. 7 (a) Linear and (b) Van't Hoff fits for C'_H *versus* temperature and inverse temperature, respectively, for H_2S (green squares), C_3H_6 (red triangles), and C_3H_8 (blue circles). Fits are shown extrapolated to (a) $C'_H = 0$ and (b) $C'_H = 1$.

Table 3 Log-modified mean absolute percentage error (MAPE) and extrapolated temperature where $C_H' = 0$ for linear and $C_H' = 1$ for Van't Hoff fits of C_H' *versus* temperature and inverse temperature, respectively

	Linear fit		Van't Hoff fit	
Gas	Modified MAPE (%)	$T_{C_H'=0}$(°C)	Modified MAPE (%)	$T_{C_H'=1}$(°C)
H_2S	3.0	132	7.8	262
C_3H_6	2.5	150	1.7	471
C_3H_8	2.4	167	0.2	1279

compared to the linear fit. The linear fits predict there to be a loss of Langmuir sorption between 132–167 °C, as is reflected in the sorption isotherms of Fig. 6 where the sorption isotherms at 190 °C exhibit negligible Langmuir contribution. As the Van't Hoff relationship does not allow for determination at $C_H' = 0$, results are reported for $C_H' = 1$. This Van't Hoff fit does not predict loss of Langmuir sorption until between 262–1279 °C. This broad range illustrates the limitations of using phenomenological models for material property predictions and corroborates conclusions by Koros and Paul[107] and Koros *et al.*[32] who determined that while the Van't Hoff fit is "convenient," it lacks theoretical justification. The linear fit, they argued, can be better related to the free volume within the polymer below its glass transition temperature and subsequent vanishing at the glass transition temperature. A comprehensive study of Xe sorption and ^{129}Xe NMR using poly(*p*-phenylene oxide) supported the observation that a linear extrapolation of C_H' to zero corroborates well with the location of the T_g, where C_H' is expected to become negligible.[109] However, extrapolations in this work do not identify a clear T_g that can be identified experimentally, as CANAL polymers do not have a detectable T_g prior to thermal degradation at ~450 °C.[5]

5.5 Sorption energetics

To better understand polymer–gas affinity between CANAL-Me-Me$_2$F and C_3H_6, C_3H_8, and H_2S, as well as to understand how these results differ from the archetypal microporous polymer, PIM-1, the thermodynamics of sorption were analyzed *via* the DMS model. The same LFER-constrained model as detailed above for CANAL-Me-Me$_2$F was used for PIM-1. The DMS parameters for H_2S in PIM-1 were computed from the isotherms of Dean *et al.*[22] The DMS parameters for C_3H_6 and C_3H_8 in PIM-1 were computed from the isotherms of Li *et al.*[110] These parameters are reported in Table S7. We note that when using an unconstrained DMS optimization, sorption energetics in PIM-1 can lead to significantly different values and trends (Table S9), thus, efforts to constrain parameters to physically-relevant trends are vital to more reliable structure–property relationships.

Langmuir sorption, as shown in Fig. 8a and Table S6, is responsible for over 55% of infinite dilution sorption at 35 °C for H_2S and over 90% for the two hydrocarbons. By 125 °C, however, these values decrease to between 25% and 65%, indicating the stronger temperature dependence of Langmuir sorption compared to Henry sorption. As shown in Fig. 8b, the sorption coefficient at infinite dilution, S_∞, of H_2S in PIM-1 has a larger contribution from the Langmuir mode than CANAL-Me-Me$_2$F. This result correlates with the lower plasticization pressure of CANALs.[19] The significantly lower S_∞ for H_2S in CANAL-Me-Me$_2$F was expected due to the degree of linearity exhibited in the isotherms shown in Fig. 6a.

As detailed explicitly in Table 4, the trends in heats of sorption differ between CANAL-Me-Me$_2$F and PIM-1. Analysis of the energetics of infinite dilution sorption for the two hydrocarbons showed that in PIM-1, C_3H_6 was significantly more exothermic than C_3H_8 ($\Delta H_{S,\infty,C_3H_6} - \Delta H_{S,\infty,C_3H_8} \approx -20$ kJ mol^{-1}) while in CANAL-Me-Me$_2$F, the two terms were nearly within uncertainty of each other ($\approx$ 1 kJ mol^{-1}). These differences in energetics between the two hydrocarbons are most significantly due to partitioning within the Langmuir

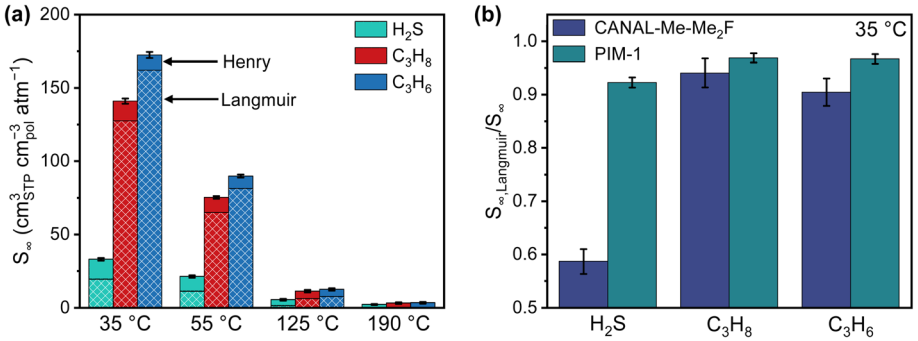

Fig. 8 (a) Sorption coefficient at infinite dilution (S_∞) for H_2S, C_3H_6, and C_3H_8 in CANAL-Me-Me$_2$F at temperatures of 35 °C, 55 °C, 125 °C, and 190 °C. Uncertainty is propagated from uncertainty in the DMS parameters and shown as the combined uncertainty of both Langmuir and Henry modes. (b) Percent contribution of S_∞ from the Langmuir mode for CANAL-Me-Me$_2$F and PIM-1, compared for H_2S, C_3H_6 and C_3H_8 at 35 °C. PIM-1 parameters were fit using previously published isotherms.[22,110]

Table 4 Heats of infinite dilution ($\Delta H_{S,\infty}$), Henry (ΔH_D), and Langmuir sorption (ΔH_b) for H_2S, C_3H_6, and C_3H_8 in CANAL-Me-Me_2F and PIM-1[22,110]

Polymer	Gas	$\Delta H_{S,\infty}$ (kJ mol^{-1})	ΔH_D (kJ mol^{-1})	ΔH_b (kJ mol^{-1})
CANAL-Me-Me_2F	H_2S	−20.5 ± 0.2	−13.6 ± 0.1	−2 ± 1
	C_3H_6	−29.0 ± 0.3	−10.9 ± 0.3	−17.0 ± 0.8
	C_3H_8	−30.0 ± 0.3	−8.2 ± 0.4	−21.7 ± 0.6
PIM-1	H_2S	−27.2 ± 0.2	−17.0 ± 0.3	−23.2 ± 0.2
	C_3H_6	−37.9 ± 0.7	−22.1 ± 0.1	−33.5 ± 0.3
	C_3H_8	−18.0 ± 0.7	−22.0 ± 0.6	−12.2 ± 0.6

regime, as differences in ΔH_D between C_3H_6 and C_3H_8 were within 3 kJ mol^{-1} for both polymers.

The differences seen in the energetics of surface sorption of C_3H_6 and C_3H_8 between CANAL-Me-Me_2F and PIM-1 are hypothesized to be due to the heteroatoms within PIM-1 that are not present in CANAL-Me-Me_2F. Propylene is more polarizable than propane, leading to potentially stronger interactions between the nitrile functionality in PIM-1 and the π-bond in propylene.[111] While no other studies on propylene sorption in CANALs have been performed, this effect can be likened to how increased side group polarity in PIM-1 (*e.g.*, conversion of nitrile groups to primary amines), increases the sorption selectivity of propylene over propane.[112] To further support the polarizability hypothesis, sorption simulations as described previously were conducted on a hypothetical CANAL-Me-Me_2F-like polymer with two methyl groups per repeat unit substituted for nitrile groups (CANAL-Me-Me_2F-CN), as shown in Fig. 9. As shown in Fig. 10, the Langmuir energetics of propylene were made more exothermic relative to propane while the Henry energetics remained similar. Details on the computational modeling of CANAL-Me-Me_2F-CN are available in Section S1.5 and DMS parameters are available in Table S8.

Similar to the previously described differences in Langmuir sorption of C_3H_6 in CANAL-Me-Me_2F and PIM-1, H_2S, as a polar molecule, demonstrates more exothermic Langmuir sorption in PIM-1 ($\Delta H_b \approx -23$ kJ mol^{-1}) than in CANAL-Me-Me_2F (≈ -2 kJ mol^{-1}). As also shown in Fig. 10, the Langmuir energetics of H_2S are more exothermic in CANAL-Me-Me_2F-CN than in CANAL-Me-Me_2F. Due to overlapping uncertainties between these energetic differences in H_2S and non-polar C_3H_8, however, these results are less conclusive than those of C_3H_6 described above.

Interestingly, ΔH_D values for all three gases in CANAL-Me-Me_2F are less exothermic than those obtained for the same gases in PIM-1. This result aligns with a previous finding that differences in sorption in the Henry's mode were strongly influenced by polymer backbone and less so on specific functionality.[22] In further agreement is that ΔH_D values between CANAL-Me-Me_2F and CANAL-Me-Me_2F-CN are within uncertainties of each other.

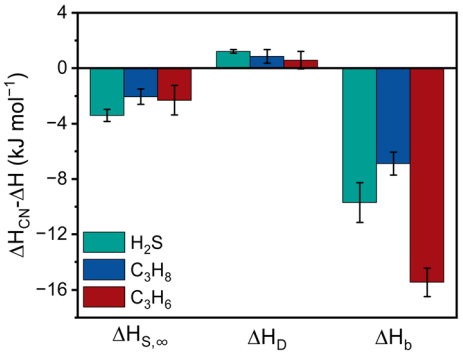

Fig. 10 Difference in heats of sorption between CANAL-Me-Me_2F-CN (ΔH_{CN}) and CANAL-Me-Me_2F (ΔH) for infinite dilution, Henry, and Langmuir sorption from constrained DMS optimization routines.

5.6 Mixed-gas sorption

To investigate the ability for CANAL-Me-Me_2F to perform the industrially relevant propylene/propane separation, the mixed-gas DMS model was applied. A 70/30 molar ratio of propylene/propane was chosen as a balance between typical hydrocarbon stream composition from catalytic cracking (>80 mol% propylene) and from propane dehydrogenation (50 mol% propylene).[113,114]

The effect of the mixed-gas DMS model on the sorption isotherms of C_3H_6 and C_3H_8 at 35 °C is shown in Fig. 11a, yielding the characteristic decrease in Langmuir capacity with unchanged sorption effects of the Henry mode, as expected from the mixed-gas model formulation. The mixed-gas selectivities in CANAL-Me-Me_2F ($\alpha^S_{C3H6/C3H8} = S_{C_3H_6}/S_{C_3H_8}$) are shown in Fig. 11b. Due to significant uncertainties in the selectivities,

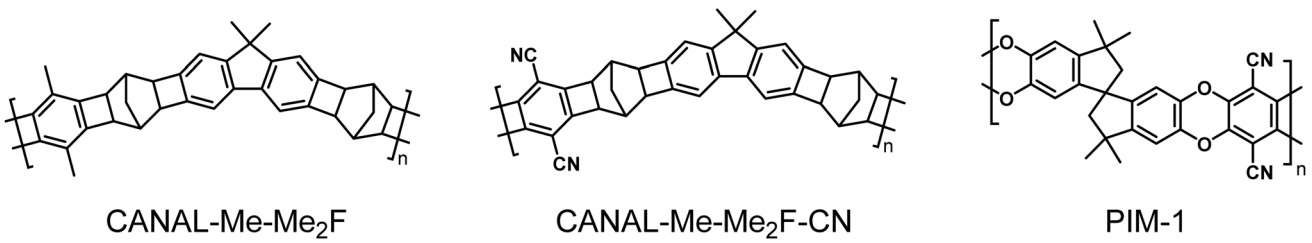

Fig. 9 Structures of CANAL-Me-Me_2F, CANAL-Me-Me_2F-CN, and PIM-1. Note that the CANAL-Me-Me_2F-CN structure is hypothetical.

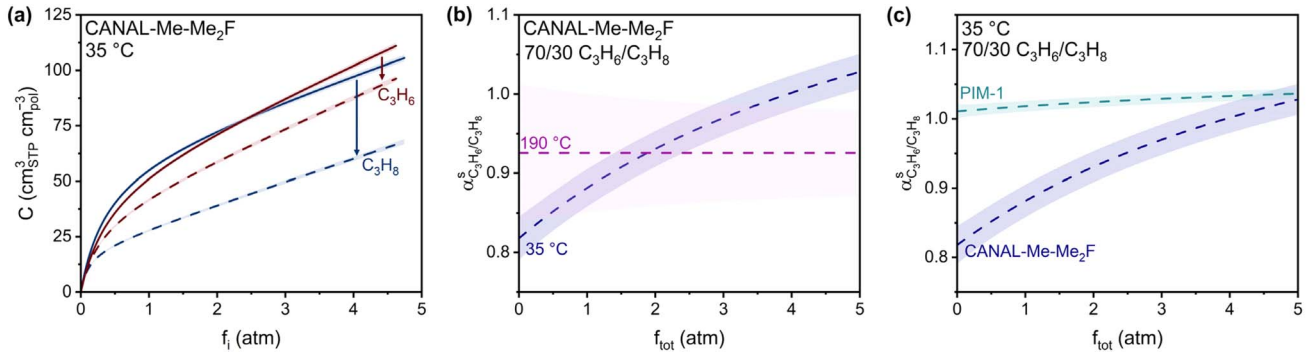

Fig. 11 (a) Dual-mode sorption (DMS) isotherms for C_3H_6 and C_3H_8 in CANAL-Me-Me_2F for pure-gas (solid lines) and mixed-gas (dashed lines) for a 70/30 molar mixture of C_3H_6/C_3H_8 at 35 °C *versus* the fugacity of each component. DMS fits were restricted *via* linear-free energy relationships (LFERs) as implemented by Wu *et al.*[29] (b) Mixed-gas sorption selectivity of a 70/30 molar mixture of C_3H_6/C_3H_8 in CANAL-Me-Me_2F at 35 °C and 190 °C *versus* the combined fugacity of both penetrants. (c) Mixed-gas sorption selectivity of a 70/30 molar mixture of C_3H_6/C_3H_8 in CANAL-Me-Me_2F and PIM-1 at 35 °C *versus* the combined fugacity of both penetrants. Data for CANAL-Me-Me_2F is from simulated MCMD isotherms. Data for PIM-1 is from the recomputed isotherms of Li *et al.*[110]

the effect of increasing temperature on selectivity from 35 °C to 190 °C cannot be definitively stated.

Comparison of the propylene/propane sorption selectivity between CANAL-Me-Me_2F and PIM-1 at 35 °C is shown in Fig. 11c. CANAL-Me-Me_2F has a sorption selectivity below one for the majority of the fugacity range studied, while PIM-1 has a sorption selectivity near one. As the Langmuir mode becomes saturated with increasing fugacity, the potential surface sorption differences between the two polymers as examined previously decrease in importance, and the propylene/propane selectivities in CANAL-Me-Me_2F and PIM-1 trend towards each other.

6. Conclusions

This study establishes an atomistic computational framework for CANAL polymers, which was validated against experimental data including density, free volume distribution (FVD), wide-angle X-ray scattering (WAXS), and sorption isotherms. Furthermore, a significant focus was placed on simulating the sorption and corresponding energetics of H_2S, C_3H_6, and C_3H_8, which are difficult to evaluate experimentally. While non-plasticizing gases were quantitatively modeled *via* GCMC, highly condensable gases—particularly the C_3H_6 and C_3H_8 hydrocarbons—required an iterative MCMD approach. These results support the use of MCMD simulations as a predictive tool, especially for time-intensive sorption studies and those with hazardous gases. Application of the dual-mode sorption (DMS) model over a broad range of temperatures from 35 °C to 190 °C for H_2S, C_3H_6, and C_3H_8 within CANAL-Me-Me_2F revealed the significant characteristic Langmuir-mode contribution to sorption at lower temperatures and pressures. By 190 °C, sorption isotherms were nearly linear and characterized by the Henry mode. The higher Langmuir affinities for the hydrocarbons relative to H_2S in the purely hydrocarbon CANAL emphasizes how sorption in the CANAL polymer is largely driven by van der Waals interactions. Langmuir energetics were more exothermic for H_2S and C_3H_6 in PIM-1 than in CANAL-Me-Me_2F, potentially due to specific gas–polymer interactions made feasible through the nitrile group present in PIM-1, which was supported by simulations of a hypothetical nitrile-functionalized CANAL-Me-Me_2F. Overall, this work advances the understanding of condensable gas sorption in high free volume heteroatom-free ladder polymers. The microstructural and multi-temperature sorption analyses performed within this study suggest that increasing size-sieving through CANAL backbone modification can be quantified *via* geometric FVDs, aromaticity can be leveraged to favor Langmuir sorption of polarizable penetrants, and temperature can be used to significantly modulate the contribution of Langmuir sorption within CANALs. By validating an atomistic simulation system for CANAL-Me-Me_2F, we provide a foundation for extending computational studies to other CANAL polymers. When used in conjunction with experiments, these simulations enable a more complete characterization of sorption behavior and support the rational design of membrane materials for complex gas separations.

Author contributions

B. C. Tapia: conceptualization, methodology, software, formal analysis, investigation, data curation, writing – original draft, visualization. J. Y. Yeo: conceptualization, methodology, formal analysis, investigation, writing – review & editing. Z. P. Smith: supervision, writing – review & editing, funding acquisition.

Conflicts of interest

Zachary P. Smith reports a relationship with Osmoses, Inc. that includes: board membership, consulting or advisory, and equity or stocks. Zachary P. Smith has patent licensed to Osmoses., Inc.

Data availability

The data supporting this article have been included as part of the supplementary information (SI). Supplementary information is available. See DOI: https://doi.org/10.1039/d5ta09448h.

Acknowledgements

The authors thank Pablo A. Dean for helpful discussions on the DMS model optimization, Cassiano G. Aimoli for helpful discussions on molecular simulations, Francesco M. Benedetti for sorption experiments of H_2, N_2, O_2, CH_4, and CO_2, and Ashley M. Robinson and Yan Xia for helpful discussions on CANAL polymer synthesis. The authors acknowledge the MIT SuperCloud, the Lincoln Laboratory Supercomputing Center, and the MIT Office of Research Computing and Data for providing HPC resources that have contributed to the research results reported within this paper. This work was supported by the U.S. Department of Energy, Office of Science, Basic Energy Sciences, Separation Science Program under Award DE-SC0023252.

References

1 D. S. Sholl and R. P. Lively, Seven chemical separations to change the world, *Nature*, 2016, **532**(7600), 435–437, DOI: 10.1038/532435a.
2 J. G. Wijmans and R. W. Baker, The solution-diffusion model: A review, *J. Membr. Sci.*, 1995, **107**(1), 1–21, DOI: 10.1016/0376-7388(95)00102-i.
3 Z.-X. Low, P. M. Budd, N. B. McKeown and D. A. Patterson, Gas permeation properties, physical aging, and its mitigation in high free volume glassy polymers, *Chem. Rev.*, 2018, **118**(12), 5871–5911, DOI: 10.1021/acs.chemrev.7b00629.
4 A. G. McDermott, P. M. Budd, N. B. McKeown, C. M. Colina and J. Runt, Physical aging of polymers of intrinsic microporosity: a SAXS/WAXS study, *J. Mater. Chem. A*, 2014, **2**(30), 11742–11752, DOI: 10.1039/c4ta02165g.
5 H. W. H. Lai, F. M. Benedetti, J. M. Ahn, A. M. Robinson, Y. Wang, I. Pinnau, Z. P. Smith and Y. Xia, Hydrocarbon ladder polymers with ultrahigh permselectivity for membrane gas separations, *Science*, 2022, **375**(6587), 1390–1392, DOI: 10.1126/science.abl7163.
6 H. B. Park, J. Kamcev, L. M. Robeson, M. Elimelech and B. D. Freeman, Maximizing the right stuff: The trade-off between membrane permeability and selectivity, *Science*, 2017, **356**(6343), eaab0530, DOI: 10.1126/science.aab0530.
7 L.-P. Guo, R.-S. Liu, J. Qian, G.-P. Hao, J. Guo, H. Wu, F. Wang and A.-H. Lu, Surface sieving carbon skins for propylene and propane separation, *Nat. Chem. Eng.*, 2024, **1**(6), 411–420, DOI: 10.1038/s44286-024-00075-9.
8 C. C. E. Christopher, A. Dutta, S. Farooq and I. A. Karimi, Process synthesis and optimization of propylene/propane separation using vapor recompression and self-heat recuperation, *Ind. Eng. Chem. Res.*, 2017, **56**(49), 14557–14564, DOI: 10.1021/acs.iecr.7b03432.
9 Physical constants of organic compounds, in *CRC Handbook of Chemistry and Physics*, ed. J. R. Rumble, CRC Press/Taylor & Francis, Boca Raton, FL, 106th edn, 2025.
10 C. Zhang, R. P. Lively, K. Zhang, J. R. Johnson, O. Karvan and W. J. Koros, Unexpected molecular sieving properties of Zeolitic Imidazolate Framework-8, *J. Phys. Chem. Lett.*, 2012, **3**(16), 2130–2134, DOI: 10.1021/jz300855a.
11 Y. Su, S. Cong, M. Shan and Y. Zhang, Enhanced propylene/propane separation in facilitated transport membranes containing multisilver complex, *AIChE J.*, 2022, **68**(1), e17410, DOI: 10.1002/aic.17410.
12 Y. H. Chan, S. S. M. Lock, M. K. Wong, C. L. Yiin, A. C. M. Loy, K. W. Cheah, S. Y. W. Chai, C. Li, B. S. How, B. L. F. Chin, Z. P. Chan and S. S. Lam, A state-of-the-art review on capture and separation of hazardous hydrogen sulfide (H_2S): Recent advances, challenges and outlook, *Environ. Pollut.*, 2022, **314**, 120219, DOI: 10.1016/j.envpol.2022.120219.
13 A. Pudi, M. Rezaei, V. Signorini, M. P. Andersson, M. G. Baschetti and S. S. Mansouri, Hydrogen sulfide capture and removal technologies: A comprehensive review of recent developments and emerging trends, *Sep. Purif. Technol.*, 2022, **298**, 121448, DOI: 10.1016/j.seppur.2022.121448.
14 T. N. A. Tengku Hassan, A. M. Shariff, M. M. Mohd Pauzi, M. S. Khidzir and A. Surmi, Insights on cryogenic distillation technology for simultaneous CO_2 and H_2S removal for sour gas fields, *Molecules*, 2022, **27**(4), 1424, DOI: 10.3390/molecules27041424.
15 F. B. Torres, J. P. Gutierrez, L. A. Ruiz, M. A. Bertuzzi and E. Erdmann, Comparative analysis of absorption, membrane, and hybrid technologies for CO_2 recovery, *J. Nat. Gas Sci. Eng.*, 2021, **94**, 104082, DOI: 10.1016/j.jngse.2021.104082.
16 X. He, D. Chen, Z. Liang and F. Yang, Insight and comparison of energy-efficient membrane processes for CO_2 capture from flue gases in power plant and energy-intensive industry, *Carbon Capture Sci. Technol.*, 2022, **2**, 100020, DOI: 10.1016/j.ccst.2021.100020.
17 K. Mizrahi Rodriguez, S. Lin, A. X. Wu, K. R. Storme, T. Joo, A. F. Grosz, N. Roy, D. Syar, F. M. Benedetti and Z. P. Smith, Penetrant-induced plasticization in microporous polymer membranes, *Chem. Soc. Rev.*, 2024, **53**(5), 2435–2529, DOI: 10.1039/d3cs00235g.
18 D. S. Sholl and R. P. Lively, Exemplar mixtures for studying complex mixture effects in practical chemical separations, *JACS Au*, 2022, **2**(2), 322–327, DOI: 10.1021/jacsau.1c00490.
19 J. Y. Yeo, F. M. Benedetti, B. Pedretti, A. M. Robinson, R. Yin, H. W. H. Lai, T. H. Lee, Y. Xia and Z. P. Smith, Investigation of competitive sorption and plasticization of hyperaged CANAL ladder polymers for acid gas purification, *J. Membr. Sci.*, 2025, **726**, 123973, DOI: 10.1016/j.memsci.2025.123973.
20 S. Yi, X. Ma, I. Pinnau and W. J. Koros, A high-performance hydroxyl-functionalized polymer of intrinsic microporosity for an environmentally attractive membrane-based approach to decontamination of sour natural gas, *J.*

Mater. Chem. A, 2015, **3**(45), 22794–22806, DOI: 10.1039/c5ta05928c.

21 S. Yi, B. Ghanem, Y. Liu, I. Pinnau and W. J. Koros, Ultraselective glassy polymer membranes with unprecedented performance for energy-efficient sour gas separation, *Sci. Adv.*, 2019, **5**(5), eaaw5459, DOI: 10.1126/sciadv.aaw5459.

22 P. A. Dean, K. Mizrahi Rodriguez, S. Guo, N. Roy, T. M. Swager and Z. P. Smith, Elucidating the role of micropore-generating backbone motifs and amine functionality on H_2S, CO_2, CH_4 and N_2 sorption, *J. Membr. Sci.*, 2024, **696**, 122465, DOI: 10.1016/j.memsci.2024.122465.

23 K. Mizrahi Rodriguez, P. A. Dean, S. Guo, N. Roy, T. M. Swager and Z. P. Smith, Elucidating the role of micropore-generating backbone motifs and amine functionality on membrane separation performance in complex mixtures, *J. Membr. Sci.*, 2024, **696**, 122464, DOI: 10.1016/j.memsci.2024.122464.

24 D. R. Paul, Effect of immobilizing adsorption on the diffusion time lag, *J. Polym. Sci., Part A-2*, 1969, **7**(10), 1811–1818, DOI: 10.1002/pol.1969.160071015.

25 G. H. Fredrickson and E. Helfand, Dual-mode transport of penetrants in glassy polymers, *Macromolecules*, 1985, **18**(11), 2201–2207, DOI: 10.1021/ma00153a024.

26 S. Kanehashi and K. Nagai, Analysis of dual-mode model parameters for gas sorption in glassy polymers, *J. Membr. Sci.*, 2005, **253**(1), 117–138, DOI: 10.1016/j.memsci.2005.01.003.

27 W. J. Koros, R. T. Chern, V. Stannett and H. B. Hopfenberg, A model for permeation of mixed gases and vapors in glassy polymers, *J. Polym. Sci., Polym. Phys. Ed.*, 1981, **19**(10), 1513–1530, DOI: 10.1002/pol.1981.180191004.

28 E. Ricci and M. G. De Angelis, Modelling mixed-gas sorption in glassy polymers for CO_2 removal: a sensitivity analysis of the dual mode sorption model, *Membranes*, 2019, **9**(1), 8, DOI: 10.3390/membranes9010008.

29 A. X. Wu, J. A. Drayton, K. Mizrahi Rodriguez, F. M. Benedetti, Q. Qian, S. Lin and Z. P. Smith, Elucidating the role of fluorine content on gas sorption properties of fluorinated polyimides, *Macromolecules*, 2021, **54**(1), 22–34, DOI: 10.1021/acs.macromol.0c01746.

30 R. M. Barrer, J. A. Barrie and N. K. Raman, Solution and diffusion in silicone rubber I—A comparison with natural rubber, *Polymer*, 1962, **3**, 595–603, DOI: 10.1016/0032-3861(62)90108-8.

31 Z. P. Smith, R. R. Tiwari, T. M. Murphy, D. F. Sanders, K. L. Gleason, D. R. Paul and B. D. Freeman, Hydrogen sorption in polymers for membrane applications, *Polymer*, 2013, **54**(12), 3026–3037, DOI: 10.1016/j.polymer.2013.04.006.

32 W. J. Koros, D. R. Paul and G. S. Huvard, Energetics of gas sorption in glassy polymers, *Polymer*, 1979, **20**(8), 956–960, DOI: 10.1016/0032-3861(79)90192-7.

33 L. J. Abbott, K. E. Hart and C. M. Colina, Polymatic: a generalized simulated polymerization algorithm for amorphous polymers, *Theor. Chem. Acc.*, 2013, **132**(3), 1334, DOI: 10.1007/s00214-013-1334-z.

34 G. S. Larsen, P. Lin, K. E. Hart and C. M. Colina, Molecular simulations of PIM-1-like polymers of intrinsic microporosity, *Macromolecules*, 2011, **44**(17), 6944–6951, DOI: 10.1021/ma200345v.

35 L. Abbott; C. Colina Polymatic: a simulated polymerization algorithm, 2013. https://nanohub.org/resources/17278, accessed 2024-11-21.

36 W. J. Morgan, D. M. Anstine and C. M. Colina, Temperature effects in flexible adsorption processes for amorphous microporous polymers, *J. Phys. Chem. B*, 2022, **126**(33), 6354–6365, DOI: 10.1021/acs.jpcb.2c04543.

37 G. Kupgan, A. G. Demidov and C. M. Colina, Plasticization behavior in polymers of intrinsic microporosity (PIM-1): A simulation study from combined Monte Carlo and molecular dynamics, *J. Membr. Sci.*, 2018, **565**, 95–103, DOI: 10.1016/j.memsci.2018.08.004.

38 D. M. Anstine, A. G. Demidov, N. F. Mendez, W. J. Morgan and C. M. Colina, Screening PIM-1 performance as a membrane for binary mixture separation of gaseous organic compounds, *J. Membr. Sci.*, 2020, **599**, 117798, DOI: 10.1016/j.memsci.2019.117798.

39 G. Kupgan, T. P. Liyana-Arachchi and C. M. Colina, NLDFT pore size distribution in amorphous microporous materials, *Langmuir*, 2017, **33**(42), 11138–11145, DOI: 10.1021/acs.langmuir.7b01961.

40 D. N. Theodorou and U. W. Suter, Detailed molecular structure of a vinyl polymer glass, *Macromolecules*, 1985, **18**(7), 1467–1478, DOI: 10.1021/ma00149a018.

41 A. P. Thompson, H. M. Aktulga, R. Berger, D. S. Bolintineanu, W. M. Brown, P. S. Crozier, P. J. in 't Veld, A. Kohlmeyer, S. G. Moore, T. D. Nguyen, R. Shan, M. J. Stevens, J. Tranchida, C. Trott and S. J. Plimpton, LAMMPS - a flexible simulation tool for particle-based materials modeling at the atomic, meso, and continuum scales, *Comput. Phys. Commun.*, 2022, **271**, 108171, DOI: 10.1016/j.cpc.2021.108171.

42 M. G. Martin and J. I. Siepmann, Transferable potentials for phase equilibria. 1. United-atom description of n-alkanes, *J. Phys. Chem. B*, 1998, **102**(14), 2569–2577, DOI: 10.1021/jp972543+.

43 M. G. Martin and J. I. Siepmann, Novel configurational-bias Monte Carlo method for branched molecules. Transferable potentials for phase equilibria. 2. United-atom description of branched alkanes, *J. Phys. Chem. B*, 1999, **103**(21), 4508–4517, DOI: 10.1021/jp984742e.

44 J.-S. Lee, C. D. Wick, J. M. Stubbs and J. I. Siepmann, Simulating the vapour–liquid equilibria of large cyclic alkanes, *Mol. Phys.*, 2005, **103**(1), 99–104, DOI: 10.1080/00268970412331303341.

45 J. Wang, R. M. Wolf, J. W. Caldwell, P. A. Kollman and D. A. Case, Development and testing of a general Amber force field, *J. Comput. Chem.*, 2004, **25**(9), 1157–1174, DOI: 10.1002/jcc.20035.

46 X. He, V. H. Man, W. Yang, T.-S. Lee and J. Wang, A fast and high-quality charge model for the next generation general

AMBER force field, *J. Chem. Phys.*, 2020, **153**(11), 114502, DOI: 10.1063/5.0019056.

47 J. J. Potoff and J. I. Siepmann, Vapor–liquid equilibria of mixtures containing alkanes, carbon dioxide, and nitrogen, *AIChE J.*, 2001, **47**(7), 1676–1682, DOI: 10.1002/aic.690470719.

48 L. Zhang and J. I. Siepmann, Direct calculation of Henry's law constants from Gibbs ensemble Monte Carlo simulations: nitrogen, oxygen, carbon dioxide and methane in ethanol, *Theor. Chem. Acc.*, 2006, **115**(5), 391–397, DOI: 10.1007/s00214-005-0073-1.

49 C. I. Bayly, P. Cieplak, W. Cornell and P. A. Kollman, A well-behaved electrostatic potential based method using charge restraints for deriving atomic charges: the RESP model, *J. Phys. Chem.*, 1993, **97**(40), 10269–10280, DOI: 10.1021/j100142a004.

50 E. Vanquelef, S. Simon, G. Marquant, E. Garcia, G. Klimerak, J. C. Delepine, P. Cieplak and F.-Y. Dupradeau, R. E. D. Server: a web service for deriving RESP and ESP charges and building force field libraries for new molecules and molecular fragments, *Nucleic Acids Res.*, 2011, **39**, W511–W517, DOI: 10.1093/nar/gkr288.

51 M. J. Frisch; G. W. Trucks; H. B. Schlegel; G. E. Scuseria; M. A. Robb; J. R. Cheeseman; G. Scalmani; V. Barone; G. A. Petersson; H. Nakatsuji; X. Li; M. Caricato; A. V. Marenich; J. Bloino; B. G. Janesko; R. Gomperts; B. Mennucci; H. P. Hratchian; J. V. Ortiz; A. F. Izmaylov; J. L. Sonnenberg; F. Williams; Ding; F. Lipparini; F. Egidi; J. Goings; B. Peng; A. Petrone; T. Henderson; D. Ranasinghe; V. G. Zakrzewski; J. Gao; N. Rega; G. Zheng; W. Liang; M. Hada; M. Ehara; K. Toyota; R. Fukuda; J. Hasegawa; M. Ishida; T. Nakajima; Y. Honda; O. Kitao; H. Nakai; T. Vreven; K. Throssell; J. A. Montgomery Jr.; J. E. Peralta; F. Ogliaro; M. J. Bearpark; J. J. Heyd; E. N. Brothers; K. N. Kudin; V. N. Staroverov; T. A. Keith; R. Kobayashi; J. Normand; K. Raghavachari; A. P. Rendell; J. C. Burant; S. S. Iyengar; J. Tomasi; M. Cossi; J. M. Millam; M. Klene; C. Adamo; R. Cammi; J. W. Ochterski; R. L. Martin; K. Morokuma; O. Farkas; J. B. Foresman; D. J. Fox *Gaussian 16 Rev. C.01*, 2016.

52 F.-Y. Dupradeau, A. Pigache, T. Zaffran, C. Savineau, R. Lelong, N. Grivel, D. Lelong, W. Rosanski, P. Cieplak and R. E. D. The, tools: advances in RESP and ESP charge derivation and force field library building, *Phys. Chem. Chem. Phys.*, 2010, **12**(28), 7821–7839, DOI: 10.1039/c0cp00111b.

53 M. L. Connolly, Analytical molecular surface calculation, *J. Appl. Crystallogr.*, 1983, **16**(5), 548–558, DOI: 10.1107/s0021889883010985.

54 C. M. Davel, T. Bernat, J. R. Wagner and M. R. Shirts, Parameterization of general organic polymers within the open force field framework, *J. Chem. Inf. Model.*, 2024, **64**(4), 1290–1305, DOI: 10.1021/acs.jcim.3c01691.

55 S. Patel and C. L. Brooks III, CHARMM fluctuating charge force field for proteins: I parameterization and application to bulk organic liquid simulations, *J. Comput. Chem.*, 2004, **25**(1), 1–16, DOI: 10.1002/jcc.10355.

56 A. S. Teja, R. J. Lee, D. Rosenthal and M. Anselme, Correlation of the critical properties of alkanes and alkanols, *Fluid Phase Equilib.*, 1990, **56**, 153–169, DOI: 10.1016/0378-3812(90)85100-o.

57 G. C. Maitland, M. Rigby, B. Smith and W. A. Wakeham, *Intermolecular Forces: Their Origin and Determination*, International Series of Monographs on Chemistry, Oxford University Press, Oxford, 1987.

58 R. W. Hockney and J. W. Eastwood, *Computer Simulation Using Particles*, CRC Press, 1988, DOI: 10.1201/9780367806934.

59 Homogeneous flows for atomic fluids: Theory, in *Nonequilibrium Molecular Dynamics: Theory, Algorithms and Applications*, ed. B. D. Todd and P. J. Daivis, Cambridge University Press, Cambridge, 2017, pp. 104–149, DOI: 10.1017/9781139017848.006.

60 W. G. Hoover, Canonical dynamics: Equilibrium phase-space distributions, *Phys. Rev. A*, 1985, **31**(3), 1695–1697, DOI: 10.1103/physreva.31.1695.

61 S. Nosé, A unified formulation of the constant temperature molecular dynamics methods, *J. Chem. Phys.*, 1984, **81**(1), 511–519, DOI: 10.1063/1.447334.

62 S. Nosé, A molecular dynamics method for simulations in the Canonical ensemble, *Mol. Phys.*, 1984, **52**(2), 255–268, DOI: 10.1080/00268978400101201.

63 M. Tuckerman, B. J. Berne and G. J. Martyna, Reversible multiple time scale molecular dynamics, *J. Chem. Phys.*, 1992, **97**(3), 1990–2001, DOI: 10.1063/1.463137.

64 L. Verlet, Computer "experiments" on classical fluids. I. Thermodynamical properties of Lennard-Jones molecules, *Phys. Rev.*, 1967, **159**(1), 98–103, DOI: 10.1103/physrev.159.98.

65 Q. Yang and C. Zhong, Molecular simulation of adsorption and diffusion of hydrogen in metal−organic frameworks, *J. Phys. Chem. B*, 2005, **109**(24), 11862–11864, DOI: 10.1021/jp051903n.

66 M. Barraco, S. Neyertz, N. E. Benes and D. Brown, Comparison of eight classical Lennard-Jones-based H_2 molecular models in the gas phase at temperatures and pressures relevant to hydrogen on-board storage tanks, *J. Phys. Chem. A*, 2023, **127**(30), 6335–6346, DOI: 10.1021/acs.jpca.3c03212.

67 M. S. Shah, M. Tsapatsis and J. I. Siepmann, Development of the transferable potentials for phase equilibria model for hydrogen sulfide, *J. Phys. Chem. B*, 2015, **119**(23), 7041–7052, DOI: 10.1021/acs.jpcb.5b02536.

68 J. K. Shah, E. Marin-Rimoldi, R. G. Mullen, B. P. Keene, S. Khan, A. S. Paluch, N. Rai, L. L. Romanielo, T. W. Rosch, B. Yoo and E. J. Maginn, Cassandra: An open source Monte Carlo package for molecular simulation, *J. Comput. Chem.*, 2017, **38**(19), 1727–1739, DOI: 10.1002/jcc.24807.

69 M. E. Fortunato, A. G. Demidov, S. Lin, P. Lin, K. Leon, B. L. A. Perera, B. C. Tapia and C. M. Colina,

SmithLabMIT/pysimm: v1.1.1, 2025, DOI: 10.5281/zenodo.17247184.

70 M. E. Fortunato; A. G. Demidov; S. Lin; P. Lin; L. Kwan; B. L. A. Perera; C. M. Colina polysimtools/pysimm, 2024. https://github.com/polysimtools/pysimm, accessed 2024-11-21.

71 M. E. Fortunato and C. M. Colina, pysimm: A python package for simulation of molecular systems, *SoftwareX*, 2017, **6**, 7–12, DOI: 10.1016/j.softx.2016.12.002.

72 A. G. Demidov, M. E. Fortunato and C. M. Colina, Update 0.2 to "pysimm: A Python package for simulation of molecular systems.", *SoftwareX*, 2018, **7**, 70–73, DOI: 10.1016/j.softx.2018.02.006.

73 A. G. Demidov, B. L. A. Perera, M. E. Fortunato, S. Lin and C. M. Colina, Update 1.1 to "pysimm: A Python package for simulation of molecular systems.", *SoftwareX*, 2021, **15**, 100749, DOI: 10.1016/j.softx.2021.100749.

74 P. R. Bevington and D. K. Robinson, *Data Reduction and Error Analysis for the Physical Sciences*, McGraw-Hill, 2003.

75 S. Neyertz and D. Brown, Single- and mixed-gas sorption in large-scale molecular models of glassy bulk polymers. Competitive sorption of a binary CH_4/N_2 and a ternary $CH_4/N_2/CO_2$ mixture in a polyimide membrane, *J. Membr. Sci.*, 2020, **614**, 118478, DOI: 10.1016/j.memsci.2020.118478.

76 C. A. Schneider, W. S. Rasband and K. W. Eliceiri, NIH Image to ImageJ: 25 years of image analysis, *Nat. Methods*, 2012, **9**(7), 671–675, DOI: 10.1038/nmeth.2089.

77 P. C. Hansen and D. P. O'Leary, The use of the L-curve in the regularization of discrete ill-posed problems, *SIAM J. Sci. Comput.*, 1993, **14**(6), 1487–1503, DOI: 10.1137/0914086.

78 K. Mizrahi Rodriguez, F. M. Benedetti, N. Roy, A. X. Wu and Z. P. Smith, Sorption-enhanced mixed-gas transport in amine functionalized polymers of intrinsic microporosity (PIMs), *J. Mater. Chem. A*, 2021, **9**(41), 23631–23642, DOI: 10.1039/d1ta06530k.

79 L. Sarkisov, R. Bueno-Perez, M. Sutharson and D. Fairen-Jimenez, Materials informatics with PoreBlazer v4.0 and the CSD MOF database, *Chem. Mater.*, 2020, **32**(23), 9849–9867, DOI: 10.1021/acs.chemmater.0c03575.

80 J.-J. Shieh and T. S. Chung, Gas permeability, diffusivity, and solubility of poly(4-vinylpyridine) film, *J. Polym. Sci., Part B: Polym. Phys.*, 1999, **37**(20), 2851–2861, DOI: 10.1002/(sici)1099-0488(19991015)37:20<2851::aid-polb5>3.0.co;2-u.

81 T. Lodge and P. C. Hiemenz, *Polymer Chemistry*, CRC Press, Taylor & Francis Group, 3rd edn, 2020.

82 Z. Tang and S. Okazaki, All-atomistic molecular dynamics study of the glass transition of amorphous polymers, *Polymer*, 2022, **254**, 125044, DOI: 10.1016/j.polymer.2022.125044.

83 M. Klajmon, V. Aulich, J. Ludík and C. Červinka, Glass transition and structure of organic polymers from all-atom molecular simulations, *Ind. Eng. Chem. Res.*, 2023, **62**(49), 21437–21448, DOI: 10.1021/acs.iecr.3c03038.

84 P. Sharma, S. Roy and H. A. Karimi-Varzaneh, Validation of force fields of rubber through glass-transition temperature calculation by microsecond atomic-scale molecular dynamics simulation, *J. Phys. Chem. B*, 2016, **120**(7), 1367–1379, DOI: 10.1021/acs.jpcb.5b10789.

85 J. Han, R. H. Gee and R. H. Boyd, Glass transition temperatures of polymers from molecular dynamics simulations, *Macromolecules*, 1994, **27**(26), 7781–7784, DOI: 10.1021/ma00104a036.

86 A. V. Lyulin, N. K. Balabaev and M. A. J. Michels, Molecular-weight and cooling-rate dependence of simulated T_g for amorphous polystyrene, *Macromolecules*, 2003, **36**(22), 8574–8575, DOI: 10.1021/ma034406i.

87 A. Karuth, A. Alesadi, W. Xia and B. Rasulev, Predicting glass transition of amorphous polymers by application of cheminformatics and molecular dynamics simulations, *Polymer*, 2021, **218**, 123495, DOI: 10.1016/j.polymer.2021.123495.

88 W. Paul and G. D. Smith, Structure and dynamics of amorphous polymers: computer simulations compared to experiment and theory, *Rep. Prog. Phys.*, 2004, **67**(7), 1117, DOI: 10.1088/0034-4885/67/7/r03.

89 L. Dubrovinsky, Thermal expansion and equation of state, in *Encyclopedia of Materials: Science and Technology*, ed. K. H. J. Buschow, R. W. Cahn, M. C. Flemings, B. Ilschner, E. J. Kramer, S. Mahajan and P. Veyssière, Elsevier, Oxford, 2002, pp. 1–4, DOI: 10.1016/b0-08-043152-6/01817-9.

90 E. A. Grulke, D. R. Bloch, A. Akihiro, J. Brandrup and H. I. Edmund, Physical constants of some important polymers, in *Polymer Handbook*, John Wiley & Sons, 1999.

91 R. F. Clash Jr and L. M. Rynkiewicz, Thermal expansion properties of plastic materials, *Ind. Eng. Chem.*, 1944, **36**(3), 279–282, DOI: 10.1021/ie50411a021.

92 M. Yamato, A. Imai and H. Kawakami, Thermal properties of polymer with intrinsic microporosity membranes, *Polymer*, 2022, **259**, 125339, DOI: 10.1016/j.polymer.2022.125339.

93 N. A. Seaton, J. P. R. B. Walton and N. Quirke, A new analysis method for the determination of the pore size distribution of porous carbons from nitrogen adsorption measurements, *Carbon*, 1989, **27**(6), 853–861, DOI: 10.1016/0008-6223(89)90035-3.

94 C. Lastoskie, K. E. Gubbins and N. Quirke, Pore size distribution analysis of microporous carbons: a density functional theory approach, *J. Phys. Chem.*, 1993, **97**(18), 4786–4796, DOI: 10.1021/j100120a035.

95 H.-G. Peng, R. S. Vallery, M. Liu, M. Skalsey and D. W. Gidley, Depth-profiled positronium annihilation lifetime spectroscopy on porous films, *Colloids Surf., A*, 2007, **300**(1), 154–161, DOI: 10.1016/j.colsurfa.2006.10.072.

96 R. Hou, S. J. D. Smith, K. Konstas, M. Doherty, C. D, C. Easton, J. Park, H. Yoon, H. Wang, D. Freeman and B. R. Hill, M. Synergistically improved PIM-1 membrane gas separation performance by PAF-1 incorporation and UV irradiation, *J. Mater. Chem. A*, 2022, **10**(18), 10107–10119, DOI: 10.1039/d2ta00138a.

97 S. Le Roux and V. Petkov, ISAACS – interactive structure analysis of amorphous and crystalline systems, *J. Appl.*

Crystallogr., 2010, **43**(1), 181–185, DOI: 10.1107/s0021889809051929.

98 L. Makowski, Characterization of proteins with wide-angle X-ray solution scattering (WAXS), *J. Struct. Funct. Genomics*, 2010, **11**(1), 9–19, DOI: 10.1007/s10969-009-9075-x.

99 J. H. Dymond, R. C. Wilhoit, K. N. Marsh and K. C. Wong, Virial coefficients of pure gases, *Landolt-Börnstein - Group IV Physical Chemistry*, ed. M. Frenkel, K. N. Marsh, Springer-Verlag, Berlin/Heidelberg, 2002; Vol. 21A, DOI: 10.1007/b71692.

100 L. Canti Theoretical modeling of gas adsorption in microporous aromatic polymers, University of Eastern Piedmont, Vercelli, Italy, 2016. doi: DOI: 10.20373/uniupo/openthesis/81935.

101 Y. Yoshimoto, Y. Tomita, K. Sato, S. Higashi, M. Yamato, S. Takagi, H. Kawakami and I. Kinefuchi, Gas adsorption and diffusion behaviors in interfacial systems composed of a polymer of intrinsic microporosity and amorphous silica: a molecular simulation study, *Langmuir*, 2022, **38**(24), 7567–7579, DOI: 10.1021/acs.langmuir.2c00661.

102 P. J. Linstrom and W. G. Mallard, The NIST Chemistry WebBook: A chemical data resource on the internet, *J. Chem. Eng. Data*, 2001, **46**(5), 1059–1063, DOI: 10.1021/je000236i.

103 D.-Y. Peng and D. B. Robinson, A new two-constant equation of state, *Ind. Eng. Chem. Fundam.*, 1976, **15**(1), 59–64, DOI: 10.1021/i160057a011.

104 M. Balçık, S. B. Tantekin-Ersolmaz, I. Pinnau and M. G. Ahunbay, CO_2/CH_4 mixed-gas separation in PIM-1 at high pressures: Bridging atomistic simulations with process modeling, *J. Membr. Sci.*, 2021, **640**, 119838, DOI: 10.1016/j.memsci.2021.119838.

105 T. H. Lee and Z. P. Smith, Better standards are needed for membrane materials, *Nat. Mater.*, 2024, **23**(1), 11–12, DOI: 10.1038/s41563-023-01763-2.

106 S. Neyertz, N. E. Benes and D. Brown, Molecular simulations of hybrid cross-linked membranes for H_2S gas separation at very high temperatures and pressure: Binary 90%/10% N_2/H_2S and CH_4/H_2S, ternary 90%/9%/1% $N_2/CO_2/H_2S$ and $CH_4/CO_2/H_2S$ mixtures, *J. Membr. Sci.*, 2023, **687**, 122092, DOI: 10.1016/j.memsci.2023.122092.

107 W. J. Koros and D. R. Paul, CO_2 sorption in poly(ethylene terephthalate) above and below the glass transition, *J. Polym. Sci., Polym. Phys. Ed.*, 1978, **16**(11), 1947–1963, DOI: 10.1002/pol.1978.180161105.

108 C. Tofallis, A better measure of relative prediction accuracy for model selection and model estimation, *J. Oper. Res. Soc. Am.*, 2015, **66**(8), 1352–1362, DOI: 10.1057/jors.2014.103.

109 H. Yoshimizu, S. Ohta, T. Asano, T. Suzuki and Y. Tsujita, Temperature dependence of the mean size of polyphenyleneoxide microvoids, as studied by Xe sorption and ^{129}Xe NMR chemical shift analyses, *Polym. J.*, 2012, **44**(8), 821–826, DOI: 10.1038/pj.2012.123.

110 P. Li, T. S. Chung and D. R. Paul, Temperature dependence of gas sorption and permeation in PIM-1, *J. Membr. Sci.*, 2014, **450**, 380–388, DOI: 10.1016/j.memsci.2013.09.030.

111 R. D. Nelson, D. R. Lide and A. A. Maryott, *Selected Values of Electric Dipole Moments for Molecules in the Gas phase, National Standards Reference Data Series; NSRDS-NBS 10*, National Institute of Standards and Technology, Gaithersburg, MD, 1967. DOI: DOI: 10.6028/NBS.NSRDS.10.

112 B. W. C. Chen and C. P. O'Brien, Highly selective propylene/propane separation using amine-modified PIM-1 (PIM-NH_2), *J. Membr. Sci.*, 2025, **731**, 124229, DOI: 10.1016/j.memsci.2025.124229.

113 W. C. Kuah, S. Effendy and S. Farooq, Industrial scale propylene/propane separation using pressure vacuum swing adsorption, *Ind. Eng. Chem. Res.*, 2018, **57**(18), 6451–6463, DOI: 10.1021/acs.iecr.8b00289.

114 S. Sridhar and A. A. Khan, Simulation studies for the separation of propylene and propane by ethylcellulose membrane, *J. Membr. Sci.*, 1999, **159**(1), 209–219, DOI: 10.1016/s0376-7388(99)00061-7.